



Performance Evaluation of FSO System under Atmospheric Turbulence and Noise

B. Sridhar¹ · S. Sridhar¹ · V. Nanchariah¹

Received: 24 July 2020 / Accepted: 4 August 2022 / Published online: 30 August 2022
© The Institution of Engineers (India) 2022

Abstract Free space optical (FSO) communication systems can be the only solution to transmit high-speed data in urban areas wireless networks. FSO communication systems are more suitable for 5G point to point communications. Performance of FSO communication systems is well-determined based on the type of modulation techniques employed as well as signal propagation under various atmospheric conditions. Proposed work is focused upon evaluating performance of FSO systems that employed OOK, BPSK, MPSK M-QAM modulation techniques in transmitters and antenna diodes (APD) in receivers. Analysis of proposed FSO communication system is carried out considering an atmospherically turbulent gamma channel model and normal (turbulence free) channel model in the case of weak/medium and strong air turbulence in air channels. The Bit Error Rate (BER) of the proposed FSO system is estimated based on various parameters like APD quantum noise, intensity of the turbulence, thermal noise of system, back ground loss, channel attenuation, link distance, etc.

Keywords Free space optical communications · Weak and strong atmospheric turbulences · Quantum Noise · Thermal and background noise · M-QAM modulation

Introduction

In the current research, the researchers are focus on optical-based systems for high data transmission. FSO has attracted great attention from industry and academia for its quick and easy implementation as an alternative solution for short-range wireless access to terrestrial communications and high data rates and cost-effectiveness. When the considered radio frequency spectrum congestion is crowded, FSO offers no license, and service feature becomes an important in modern communication networks. Attenuation and turbulence are the two main factors that degrade system performance in FSO ground communications. The absorption and dispersion process is variable and difficult to predict the atmospheric attenuation, which greatly limits the scope of application of the FSO system. Atmospheric turbulence is an occurrence of a change in the refractive index due to a lack of uniformity in temperature and pressure changes [1–12, 21, 22].

The approximation of the Gaussian Q function provides strict limits for all current exponential approximations. This approximation obtained using the binomial approximation of Q function provided by Olabiyi et al. was used [6]. In recent years, the BER of BW-impaired OWC systems has been described by Chiani et al. [7]. However, none of these studies provided a closed representation of BER under weak disturbance that facilitated the calculation of BER for a broader category of modulation schemes. Therefore, it is important to have a formal closed analytical expression to simplify the BER investigation. Hassan et.al sequential extension of the modified Bessel function was used to derive the symbol error rate (ASER) closed-circuit representation of the gamma and gamma distribution and negative exponential channels. In this work, electrical signal-to-noise ratio (SNR) was also described as a function of backlight and

✉ B. Sridhar
srib105@gmail.com

¹ Department of Electronics and Communication Engineering, Lendi Institute of Engineering and Technology, Vizianagaram, India

thermal noise, an ASER to SNR assay of turbulent channels in the atmosphere was performed without consideration of the effect of noise reception. In addition, all studies ignored the effects of cohesive damage, including environmental mitigation and technical damage [1].

In this work, the authors have estimated the bit error rate (BER) of the FSO system under conditions of weak air turbulence along with quantum noise, thermal noise and other background noises with consideration of various schemes of modulation techniques. Since FSO system a high power LD/LED source transmitters are used, operating at high frequencies the peaks of quantum power spectral density, thermal power generation over the substrate of the receiver also considered. The proposed work performance of system BER with respect to individual noise sources and total noise sources is calculated with consideration of modulation scheme, and the performance is also estimated with pin photo and avalanche photodiode by choosing their various different responsive values. In section II, the block diagram of FSO and various modulation schemes are discussed. In section III, performance parameters of FSO systems and theoretical details are discussed. In section IV, the results are analyzed and the noise dominance in various modulation schemes is compared, and finally the conclusions are given in the proposed work.

FSO Modulation Schemes

FSO block diagram is shown in Fig. 1 which consists two parts, namely electrical signal system part and optical signal systems part. In electrical part, high data are

accumulated by using various electrical parts as shown in Fig. 1. Optical signal part consists of optical sources such as LED/LD, detectors (APD) and focus lens. In general, FSO system are installed for the purpose of short-distance communication with huge data rate transmission. BER of the all effects all subsystems, such as especially receiver characteristics and channel characteristics [2].

This irregularity of the indicator can increase BER and decrease the quality of the received signal of the FSO system. Generally, OOK (on/off keying) is a low-cost FSO systems initially implemented easily in fields. In the OOK schemes, the BER can be improved by adjust the threshold of the receiver. However, due to the differences in signal strength, adjustment threshold is difficult to achieve. In addition, an alternative modulation technique has been proposed for FSO connections, phase shift keying (PSK) which is extremely energy efficient compared to OOK but the bandwidth performance is poor. Transcending the boundaries of PSK and OOK, the carrier phase shift (PSK) mechanism has been extensively studied. The classic and widely used modification techniques used in FSO are OOK scheme. The performance of OOK-FSO is not much better with a fixed detection threshold in turbulent weather conditions. In order for the OOK-FSO linker to show optimum performance in turbulent weather conditions, the threshold level must be changed according to typical lighting fluctuations and noise from incoming optical radiation. It is not possible to determine the range of adaptation as it requires optical components and constant monitoring of weather conditions. PSK-based FSO systems do not require a threshold value. To improve the quality of transmission and average BER, a M-PSK plan was developed to

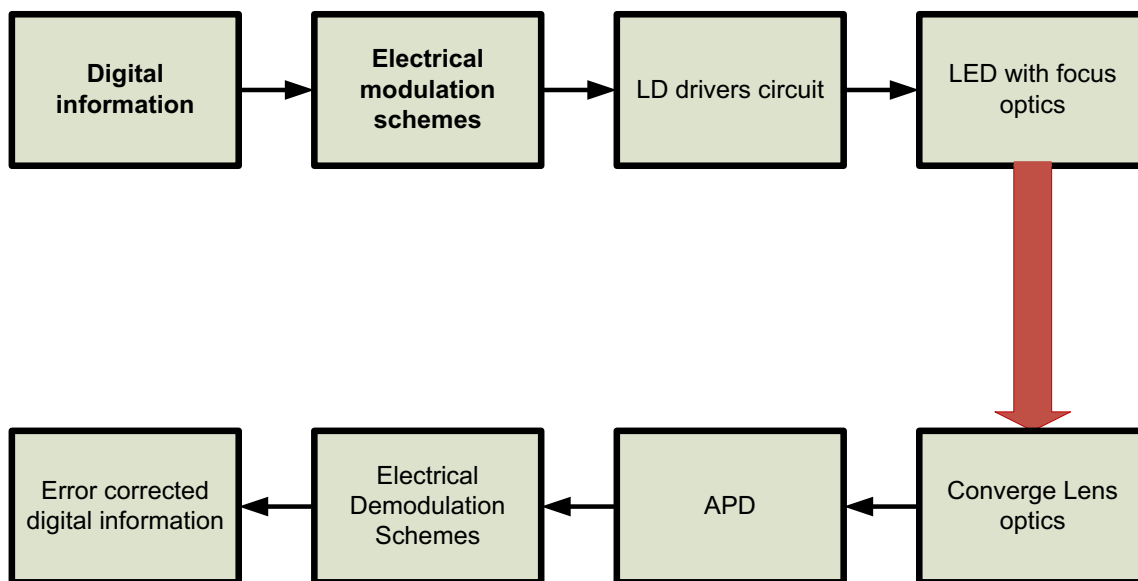


Fig. 1 Block diagram of FSO system

increase the data rate, but a level of maximum adaptation was developed to improve BER [3, 4].

Moreover, to achieve better spectral efficiency, a sub-carrier amplitude (QAM) modulation is proposed and implemented in FSO system than the M-PSK. FSO system that uses the QAM modulation square with the subcarrier density of the normal logarithmic and turbulent gamma channels is obtained symbol error rate (ASER) [5].

The modification of sub-carrier intensity (SIM) is not affected by the effects of amplitude fluctuations due to the disturbance, and it also does not require adaptive thresholds and uses a channel bandwidth that is much lower than OOK, but has a high peak-to-peak ratio. Average ratio (PAPR) with a little energy efficiency is important to note that OOK devices require complex transceiver designs due to timing and high bandwidth requirements. This study examines, among other things, the performance of approved OOK-scheme and other FSO connections in adverse weather conditions (e.g., log normals, gamma ovens, and negative expansion channels) [4].

FSO System Performance Evaluation Parameters

The BER is a key parameter for evaluating the performance of communication systems through fading channels. The analytical evaluation of the average BER for a troubled, weak FSO system is very difficult because it involves the statistical mean of the BER at the natural logarithmic distribution. The instantaneous BER of different modulation patterns in the FSO system is indicated by the Gaussian Q function, $Q(x)$. Therefore, for weak atmospheric turbulence, the OWC BER account includes complex integrations associated with $Q(x)$ and regular PDFs. Because it is difficult to deal mathematically with the closed representation of these integrals, it is difficult to analyze the bit error performance analytically. Therefore, the average rate is calculated. Thus, the BER of the FSO system for various modulation patterns is calculated under generally weak turbulent conditions using Gauss–Hermite (GH) squared numerical methods, Rytov scatter approximation and Monte Carlo simulation [2].

Given the complexity of the analysis associated with the exact mathematical expression of $Q(x)$, it is difficult to obtain a closed representation of BER. However, the simple and strict approximation of the Gaussian function $Q(x)$ can facilitate induction of closed morphological representation of mean error rate [3].

The first approximation is obtained using point estimates from a regular PDF file. Additionally, closed approximation is derived using the Taylor Accessory Series to approximate natural logarithmic integration, which is not only mathematically manageable, but also general enough to evaluate the

BER for modulation diagrams for various formation widely used in weak weather disturbances. Theoretical study on channel modeling with considerations un favor conditions, quantum noises at front end of the receiver and thermal noise with all conditions of receiver and channel are described below.

Channel Model

The signal propagated through the FSO channel effects or distorted by various atmospheric interference dispersion, scattering due to rain, dust, fog, amplitude and phase of the traffic signal, that is, atmospheric attenuation, transmission loss and atmospheric turbulence factors characterize the FSO channel. For atmospheric turbulence, normal logarithmic models and gamma models are considered weak/medium and strong atmospheric gases [3].

Channel loss consists of a turbulent atmosphere and an engineering loss. The molecular absorption and dispersion of suspended aerosols in the air are generated atmospheric damping, engineering loss also obtained by different tilt angle of diffuser and receiver opening area. Mathematically, let us consider the A_v represented as:

$$A_v = \frac{A}{\pi \left(\frac{\theta L}{2}\right)^2} e^{-\beta_v L} \tag{1}$$

where the coefficient of atmospheric absorption, the distance of the link between the area of the transmitter and receiver, the optical receiver and the angle of change (radians) are indicated as: β_v, L, A and Θ [3].

Disturbance model is also considered; when a traffic signal is spread through the FSO channel, Xt scintillation provides a steady random process. Assume that the mean flashes in the normal logarithmic turbulent channel are normalized to 1[4]:

Described as probability density function (PDF) for $f_x(X)$.

$$f_x(x) = \frac{1}{x\sigma_s\sqrt{2\pi}} \exp \frac{-\left[\ln(x) + \frac{\sigma_s}{2}\right]^2}{2\sigma_s^2} \tag{2}$$

The luminescence index is Cith σ^2 , which can vary with the channel characteristics. The equation is as follows:

$$\sigma_s^2 = Exp \left[\frac{0.49\sigma_2^2}{(1 + 0.18d^2 + 0.56\sigma_2^{12/5})^{2/3}} + \frac{0.51\sigma_2^2(1 + 0.69\sigma_2^{12/5})^{-5/6}}{(1 + 0.9d^2 + 0.62d^2\sigma_5^{12/5})} \right] - 1 \tag{3}$$

where d depends on the bonding distance L, $d = kD \times 4L$ p and $k = 2\pi\lambda$ depends on the opening diameter of the receiver.

Rytov scatter for square wave propagation is

$$\sigma_2^2 = 0.49C_n^2 k^{7/6} L^{11/6} \tag{4}$$

where C_n^2 gives the severity of the disturbance. In general, the horizontal paths up to a few kilometers variation of C_n^2 is constant. During stronger disturbance, the normal logarithmic distribution causes a considerable variation from the tentative results. Since the PDF lognormal function reduces the performance of the line compared to the measured results [7],

the PDF of gamma-gamma channel model is given as $f_X(X)$:

$$f_X(x) = \frac{2(\alpha\beta)^{1+(\alpha+\beta)/2}}{\Gamma(\alpha)\Gamma(\beta)} x^{(\frac{\alpha+\beta}{2})-1} K_{\alpha-\beta} \left(2\sqrt{\alpha\beta}x \right) \tag{5}$$

where $K_i \bullet$ is a modified type II and system Bessel function represents the gamma function is $\Gamma \bullet$. When considered the square wave propagation in channel, the α and β can be expressed by Rytov approximation shown as:

$$\alpha = \left\{ \exp \left[\frac{0.49\sigma_2^2}{\left(1 + 0.18d^2 + 0.56\sigma_2^{12/5} \right)^{7/5}} \right] - 1 \right\}^{-1} \tag{6}$$

$$\beta = \left\{ \exp \left[\frac{0.51\sigma_2^2 \left(1 + 0.69\sigma_2^{12/5} \right)^{-5/6}}{\left(1 + 0.9d^2 + 0.62d^2\sigma_2^{12/5} \right)} \right] - 1 \right\}^{-1} \tag{7}$$

A General Solution to Compute the Integral Number of the Gauss–Hermite Quadratic Approach is Presented

$$\int_{-\infty}^{\infty} e^{-x^2} f(x) dx = \sum_{i=1}^n f(x_i) + R_n \tag{8}$$

where n is the number of sample points used for rounding. x_i is the root of $H_n(x)$ ($i = 1, 2, \dots, n$). This is a notification $2^{n-1} n! \sqrt{\pi/n^2} H_{n-1}^2(x_i)$ from the relevant w_i and provided by R_n . $(2n) f$ is the second derivative of f and ξ is a number between $-\infty$ and ∞ . In general, the exact value of R_n is unknown, $f^{2n}(\xi) \sqrt{\pi/2^n} (2n)!$, but the form of its analysis is generally known R_n . It can be used to set the upper limit of n in terms of [11, 20].

Abramovitch et al. [12] provide a table and portion for weight up to $n = 20$. Using this equation, BER can be approximated as follows:

The instant BER of the optical wireless channel can be expressed to the instant SNR.

$$P_{e,L,n}(\gamma_G, \sigma_s) \cong \frac{1}{2\sqrt{\pi}} \sum_{i=1}^n W_i \operatorname{erfc} \left[\sqrt{\gamma_G/2} e^{\sqrt{2\sigma_s x_i - 2\sigma_s^2}} \right] \tag{9}$$

When considering the overall FSO system, the received power P_R is

$$P_R = P_T * H_O \tag{9A}$$

Consider light energy transmitted to the LED is P_t , and H_O channel model which obtain the Fourier transform convolution of atmospheric turbulences which is given above equation. Total received power including noise power N generates by the FSO system [2, 19].

$$Y_R = P_T * H_O + N \tag{10}$$

Here N is the noise power, responsivity of the photodiode is R , then received power at receiver is denoted as Y_R .

The current FSO communication system’s received signal power can be represented as

$$Y = R * I * H_O + N \tag{11}$$

Here, normalized irradiance or intensity (I) is based on random variations channel condition. The irradiance fluctuations are modeled with consideration of atmospheric weak, and strong turbulence a log-normal distribution is represent with PDF [4]

Then, the estimated output of receiver is given as

$$\bar{Y} = \frac{RE(I)^2}{N} \tag{12}$$

AWGN should be added to the white Gaussian noise. However, the noise power precisely calculated with material and various parameters to be considered.

The LPS performance noise is mainly caused by the channel and receiver noise, and it is related to the operating noise and the thermal noise (other noise is ignored). Total noise contrast is given as follows:

$$\sigma_{total}^2 = \sigma_{shot}^2 + \sigma_{thermal}^2 \tag{13}$$

Quantum Noise

Quantum noise is generated in the photodiode due random fluctuations of photons within an optical field that limits the sensitivity of the diode. In particular, random fluctuations exert amplitude variations effect on the photodiode to induce quantum radiation pressure noise and phase fluctuations produce trigger noise. The power spectral density leads to standard quantum limits (SQL) with two types of quantum noise are not correlated [3, 18]

$$S_{hh}^{SQL}(\Omega) = \frac{8h}{2\pi M \Omega^2 L^2} \tag{14}$$

If the random signal has an angular frequency Ω , M and L are the mass and length of the photodetector. However,

SQL is a not actual limitation for operation of photodiode. It can handle a wide variety of QND (column demolition) systems. These techniques generally include modifying the optical configuration of the photodetector that generates current by inserting additional optical filters. The focused lens can act as passive Fabry–Perot cavities, and as filter, it can be considered active cavities with external power input.

In the optical channel, the transmission quality is usually affected by the imaging noise, which mainly occurs by reference of incident light and ambient light. Shooting dispersion

$$\sigma_{shot}^2 = 2qRP_rB + 2qI_{bg}I_2B \tag{15}$$

Since ‘q’ and I_{bg} represents the electron’s charge and background current, B, I_2 are the channel bandwidth and noise bandwidth factor.

Thermal Background Noise

Modern IR (infrared medium) detector (such as PbS, PbSe, InSb, and HgCdTe) are major challenges due to their intrinsic thermal background at low-band detector radiation itself. But researchers are promising frequency conversion detector (UCD) capable of operating at room temperature an alternative to traditional direct detection at low noise level available with UCD silicon/CCD for improved SNR [13, 14, 17].

In order to estimate the equivalent noise power limits for UCD systems, it is necessary to evaluate the nonlinear materials themselves [15].

It is assumed the azimuth symmetry of the upward conversion by combining the equation. L is the length of device, for φ_{IR} at $0-2\pi$ angle. ‘c’ is the velocity of light, n'_{IR} noise at infrared wavelength λ_{IR} , and ‘h’ is the planks constant. To calculate the refraction equation, the Selmer equation is used according to temperature and wavelength. As the authors have considered the interaction between the lines of the participating waves, each refractive index is also taken into account, since all waves are strongly polarized. Interactive wave’s Δk value can vary with the angles T and φ and claim the ‘sin’ function in the equation. This is an important factor in determining the changed spectral bandwidth and acceptable angles (IR and IR). Finally, the total thermal radiative power is

$$P_{thermal}^{sp} = \frac{hc^2\alpha(\lambda_{IR})}{\lambda_{IR}^5 \exp\left[\frac{(hc)}{\lambda_{IR}K_B T} - 1\right]} \left[\frac{8\pi^2 d_{eff}^2 PL^2 Z_o}{\lambda_{IR}^2} \right] X(\theta_{ir}, \varphi_{ir}, z) \tag{16}$$

where

$$X(\theta_{ir}, \varphi_{ir}, z) = \iiint_{Z\varphi_{ir}\theta_{ir}} \left[\left(\frac{n_{IR}}{n_{upn\varphi}} \right) \left(\frac{L-z}{L} \right)^2 e^{-\left(\frac{\alpha(\lambda_{IR})(L-z)}{2} \right)} \left\{ \frac{\sinh^2\left(\frac{\alpha(\lambda_{IR})(L-z)}{4} \right) + \sinh^2\left(\frac{\Delta k(L-z)}{4} \right)}{\left(\frac{\alpha(\lambda_{IR})(L-z)}{4} \right) + \left(\frac{\Delta k(L-z)}{4} \right)} \right\} \right] \sin\theta_{ir} d\theta_{ir} d\varphi_{ir} dz$$

However, the thermal noise is considered as the current generated by the power $P_{thermal}^{sp}$ irradiated by the infrared detector [4].

Thermal noise is mainly caused by the receiver amplifier, whose deviation is:

$$\sigma_{thermal}^2 = \frac{8\pi k T k}{G} \eta A I_2 B^2 + \frac{16\pi^2 k T T_k}{G} \eta A I_2 B^2 \tag{17}$$

where G, T_K , η , K are the open-loop voltage gain, absolute temperature, fixed capacitance of the detector per unit area, and Boltzmann constant, respectively. When the system is MOSFET-based, then channel value gm (conduction) and Γ is the noise coefficient, B is the noise bandwidth factor for light distribution received at infrared region.

Numerical Results and Discussions

The FSO link shown in Fig. 1 developed as mathematical modeling which includes powers budget equations. All quantities are expressed in the modeling equation is average values. The link parameters are taken and depend on real-time scenario shown in Table 1. These parameter effects are analyzed in this section. Table 1 include various types of atmospheric turbulences and sun and sky irradianations at given wavelengths in infrared region, i.e., 850/1100/1550 nm. Simulation results are analyzed at various temperature conditions.

The BER FSO system is calculated using the proposed approximate formula for various modulation schemes. Results are obtained using Gauss–Hell approximation for order 20 and simulation of Monte Carlo and compared. There are over 100 independent iterations in Monte Carlo simulations performing a logarithmic optical channel. Symbol rate $R_b = 150$ Mbps; Responsivity $R = 100$ of a detector, Modulation index from 1 to 10, Subcarrier signal amplitude A, Load resistance detectors RL 50 Ohms Ambient temperature $Temp = 300$ K; Background noise considering 1 cm^2 receiving aperture at optical source wavelength 850 nm.

Sky radiation noise = 10^{-3} W/cm²-um-sr at 850 nm wavelength, in sun radiation noise in W/cm²-um = 550×10^{-4} at 850 nm wavelength; in radian optical filter bandwidth in 10^{-3} μm field of view (FOV) 0.6. The Rytov differences consequent are 0.023, 0.101, 0.3 and 0.6017. This

Table 1 Experimental parameters

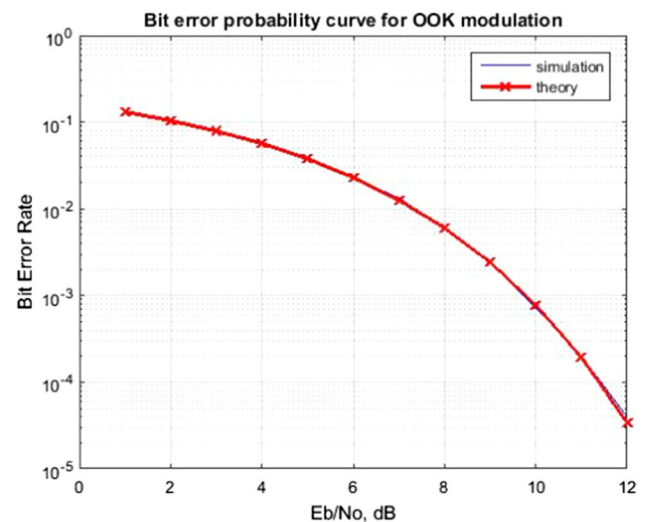
Parameter	Value	
Laser diode/LED	Peak wavelength	850 nm/1100/1550
	Transmitted optical power	10 smW
	Maximum peak-to-peak voltage	500 mV
	Beam divergence	Less than 10
	Field of view(FOV)	0.6
Transmitter considerations	Type of modulation	16-QAM
	Symbols rate	155 GB
	Optical filter bandwidth	10^{-3} um
	Refractive index structure parameter	0.75×10^{-14}
	FOV	0.6
Photodetector	Responsivity	1–100
	Load resistance	50
	Temperature	300 k
	Spectral sensitivity @ 850 nm	0.59 A/W
	Rise and fall time	5 ns Max
	reversed bias voltage	40 V
Channel consideration	Sky irradiations	10^{-3} W/cm ² -um-sr
	Sun irradiations	550×10^{-4} W/cm ² -um
	Range	1 km
	Temperatures	273/300/310 K

value is suitable for unstable conditions such as natural logarithmic distribution. For FSO system analysis, LPS $L = 1$ km is taken into account at the operating wavelength $h = 850$ nm. Cn^2 values are determined as follows: $4.2 \times 10^{-16} \text{ m}^{-2/3}$, $1.4 \times 10^{-15} \text{ m}^{-2/3}$, $4.2 \times 10^{-15} \text{ m}^{-2/3}$ and $8.4 \times 10^{-15} \text{ m}^{-2/3}$.

The Gauss–Hermite field is a numerical method and its accuracy depends on the number of digits received (i.e., N). It is computationally intense because it also includes counting corresponding weights and zeros. Nevertheless, the proposed representation is a simple and closed approach to FSO bit rate assessment. It is common to evaluate the BER for the various modulation schemes widely used in weak weather disturbances. Furthermore, Gauss–Hermite squared the representation which can not only retain great accuracy, but also manage analytically.

In Fig. 2, the BER of the proposed OOK structure is expressed as the average signal-to-sound ratio (SNR) of the OOK modulation when the number of transmitters and receivers is $M = N = 5$.

This decrease continues until true particular changes in the other average power values, but increases as average power increases. Without adjusting system parameters, this can lead to improve the performance of FSO system. Figure 2 shows a graph of the BER adjustment versus the OOK adjustment versus the SNR average of the FSO association obtained using the closed formal expression. However, some trade-offs with results obtained using Gauss–Hermite convergence and Monte Carlo models can

**Fig. 2** OOK modulation FSO system characteristics BER vs SNR

be seen in systems with high signal-to-noise ratio and high turbulence. But, the specificity of the graphs obtained using the equations is similar to that obtained using the Gauss–Hermite approximation, as well as Monte Carlo simulations. [1].

The accuracy of the proposed representation results in the high SNR region can be achieved with an increase in the number of block points. It has been noted that for large SNR ranges, the results obtained using the suggested expression exactly coincide with the exact values at low Cn^2 values.

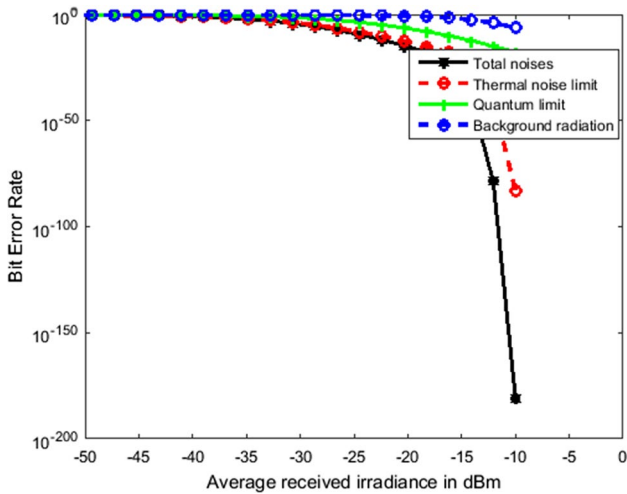


Fig. 3 BPSK FSO system characteristics average irradiance VS BER

Figure 3 shows BER performance for SIM-BPSK charts using average irradiance. Note that for large ranges of signal-to-noise ratio, the results obtained using the proposed expression correspond to the correct values of the lower values of Cn_2 . Figure 4 depicts a graph corresponding to BER for modifying SIM-BPSK based on the proposed representation. As expected, an increase in turbulence intensity is observed in Fig. 3 and Fig. 4 as a decrease in system performance. The figure shows the effect of quantum noise and background thermal noises. In the proposed experiment, quantum noise is negligible at various irradiance values; however, thermal noise is more dominant along with atmospheric turbulence as shown in Fig. 4.

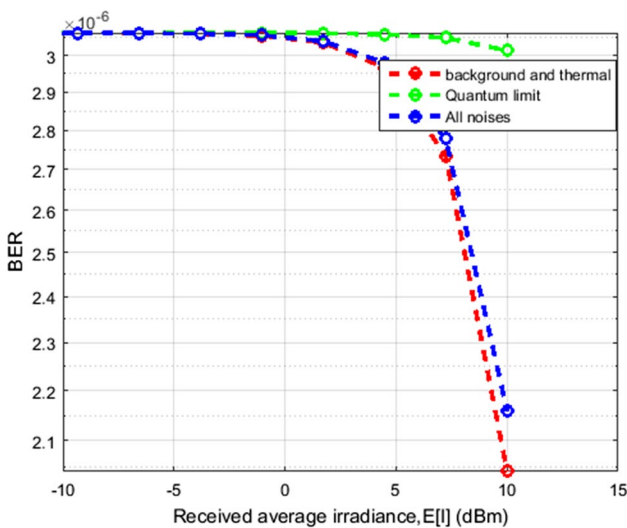


Fig. 4 BPSK FSO system characteristics average irradiance VS BER

In Fig. 3, the equation has been generated BER for FSO link at various levels of environmental exposure and ignore the simple compatibility that arises during the experiment. In the case of strong turbulence, the increase in cocking error leads to a significant increase in FSO BER. Moreover, even in moderate disturbances, correction errors have a significant impact on the performance of FSO BER in terms of increasing the bit error rate [10].

Also consider the correlation range of ABER at by AWGN under weak strong turbulent conditions in the EW fading channel. BER is limited to the operating noise of Q in various turbulent conditions using (9) and (10) in the fading channel EW. The analytical results for the limit of the union are well-aligned with the MC simulation, which indicates that the analytical results for BER can be a good prediction of the real situation. Moreover, the opening average has a clear effect on BER to BER for distributing cyber warfare in robust turbulent conditions compared to weak turbulence conditions and is the same as OOK and BPSK modifications [11, 22].

The figure shows the effect of quantum noise and background thermal noises. In the proposed experiment, quantum noise is negligible at various irradiance values; however, thermal noise more dominant along with atmospheric turbulence is shown in Fig. 4.

The results indicate that when the maximum power remains constant, the average received power decreases with an increase in M-array, which affects the performance of the system, so that with increasing M, the performance of BER decreases.

In addition, the OOK system shows less performance with FSO system than SIM-BPSK system.

The change in the bit error rate in the MPSK and MQAM diagrams is shown in Fig. 5 for the average signal-to-error

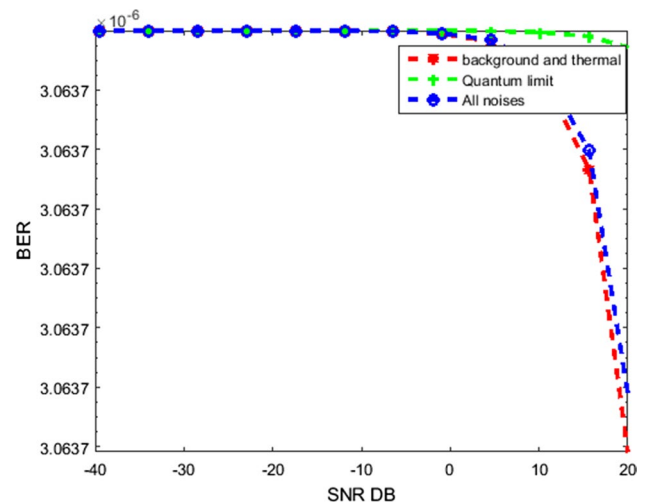


Fig. 5 MPSK FSO system characteristics SNR VS BER

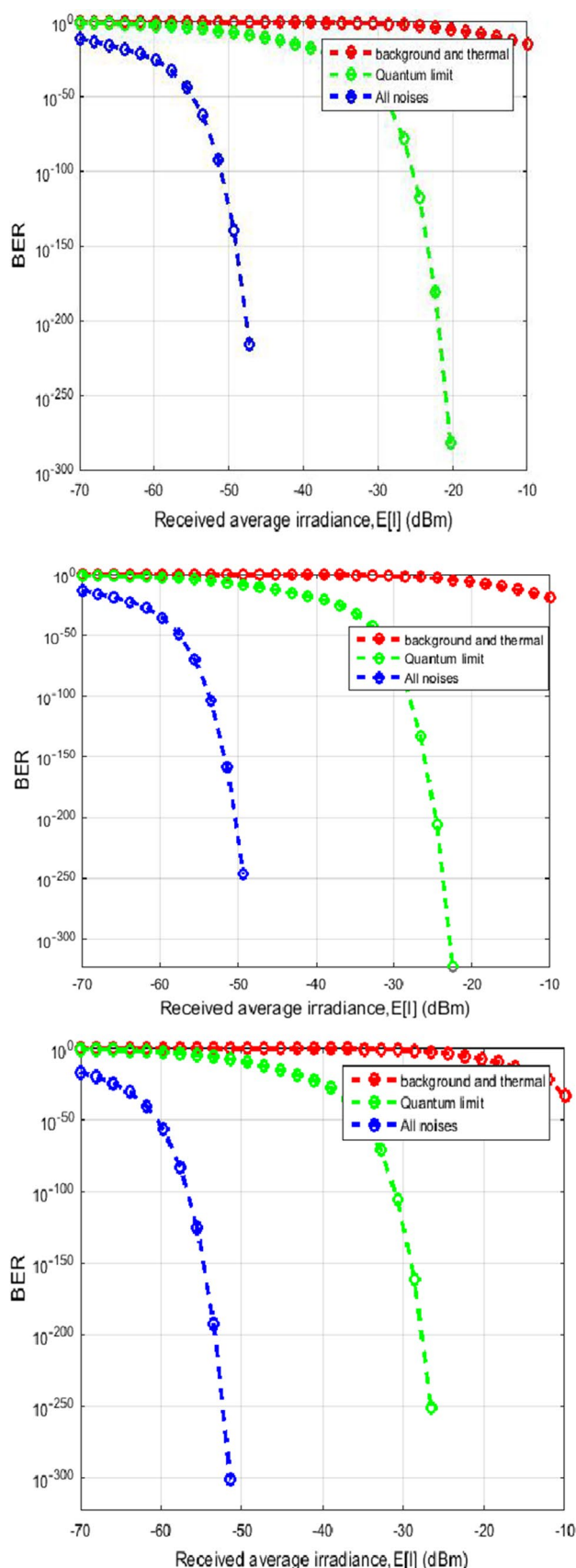
Fig. 6 **A** QAM FSO system characteristics average irradiance VS BER (i) 850 (ii) 1100 (c) 1550 nm, **B** QAM FSO system characteristics average irradiance VS BER (i) 272 K (ii) 300 K (c) 310 K

ratio for the various values of M , and here considered as $C_n^2 = 1.4 \times 10^{-15}$. As expected, BER performance decreases as M values for PSK and QAM increase. MQAM outperforms MPSK for large, medium to high M as shown in Fig. 6. BER value largely depends on operating wavelength of LED source and absolute temperature of the atmospherics. To analyze that FSO is experimented with 850/1100/1550 nm operating LED, and simulated with different various temperatures 273 K/300/310 K, the results are shown in Figs. 6 and 7. It can be seen that the graph obtained with the proposed representation closely coincides with the graph obtained with the Gauss–Hermit approximation and Monte Carlo simulation [6].

Figures 6 and 7 show the effect of quantum noise and background thermal noises. In the proposed experiment, quantum noise effects at minimum level when compared to thermal noise, where thermal noise effect is negligible at various irradiance values. However, thermal noise less dominant along with atmospheric turbulence is shown in Fig. 6, and quantum noise moderately effects on overall performance of the FSO system. MQAM proposed method results observe that overall noise in receiver by the atmospheric turbulence is more dominant, and minimizes the internal effects of the system. As shown in Fig. 6 at given $M = 8$, BER of FSO system uses QAM high value and reduces all internal noises and moderately minimizes channel noise. When compared to the all modulations schemes, MQAM gives the better performance high BER value compared to the M-PSK, BPSK-OOK schemes. However, the design of the system is more complex when compared to other systems [4, 6, 16].

The results indicate that when the maximum power remains constant, the average received power decreases with an increase in M -array, which affects the performance of the system, so that with increasing M , the performance of BER decreases [4, 12].

The low atmospheric turbulence transmission channel was used to describe the medium and severe turbulence transmission channel using Monte Carlo simulation model. When the simulation is performed, a decrease in the average bit error rate and increase in the average capacity are obtained in order to increase the average electrical signal-to-noise ratio. The average BER increases and throughput increases for strong turbulent FSO. This behavior and strength of turbulence of atmosphere are estimated with stable structure of model. Here, higher stability structure increases by increase in Rytov variation that results FSO system to generate an increase in BER and decrease in the channel capacity. Turbulence randomly changes with nonlinear variation of medium is increases. If the authors



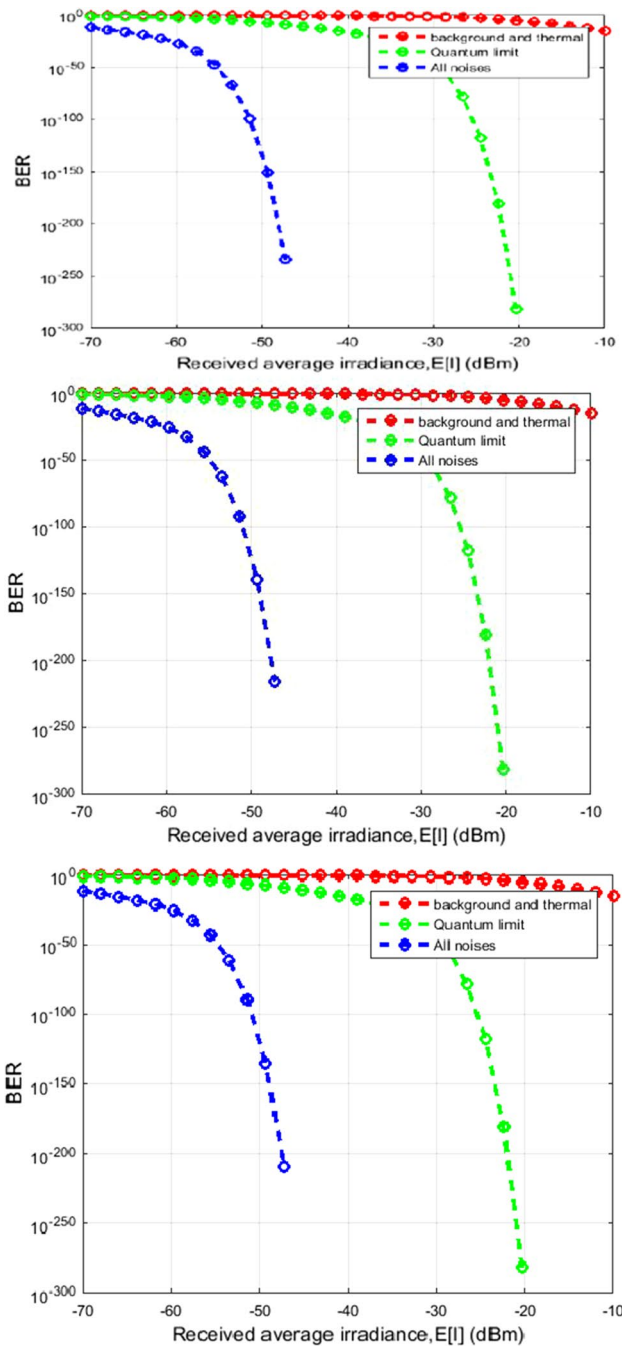


Fig. 6 (continued)

have considered the wavelength of the optical source is changed, then the average BER is also varied. If increase in the wavelength of the source results in decrease in average BER, then average capacity of the optical link changes. Simulation results also show low power of source, and the length of link is too long that effects the average capacity, and BER decreases.

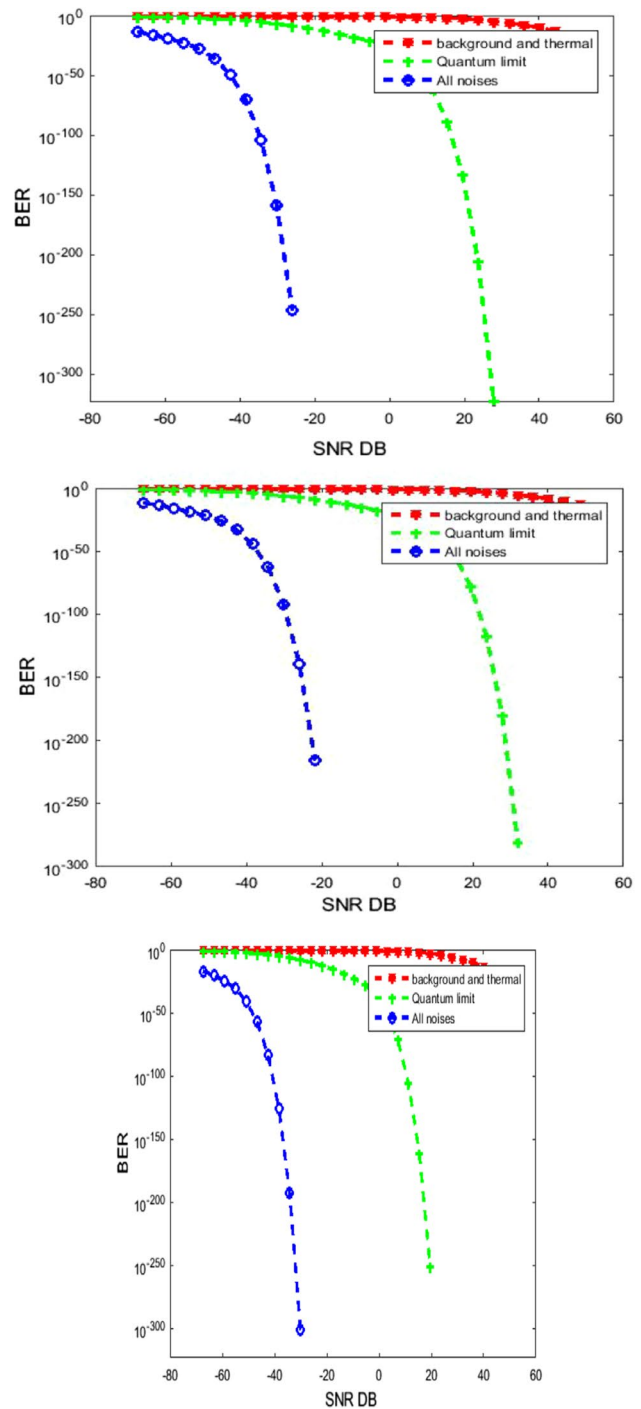


Fig. 7 A QAM FSO system characteristics SNR VS BER (i) 850 (ii) 1100 (c) 1550 nm, B QAM FSO system characteristics SNRVs BER (i) 272 K (ii) 300 K (c) 310 K

Conclusion

The proposed work predominantly focused upon analyzing the effects of inappropriate atmospheric fading and its impact on the behavior of FSO system typically employing

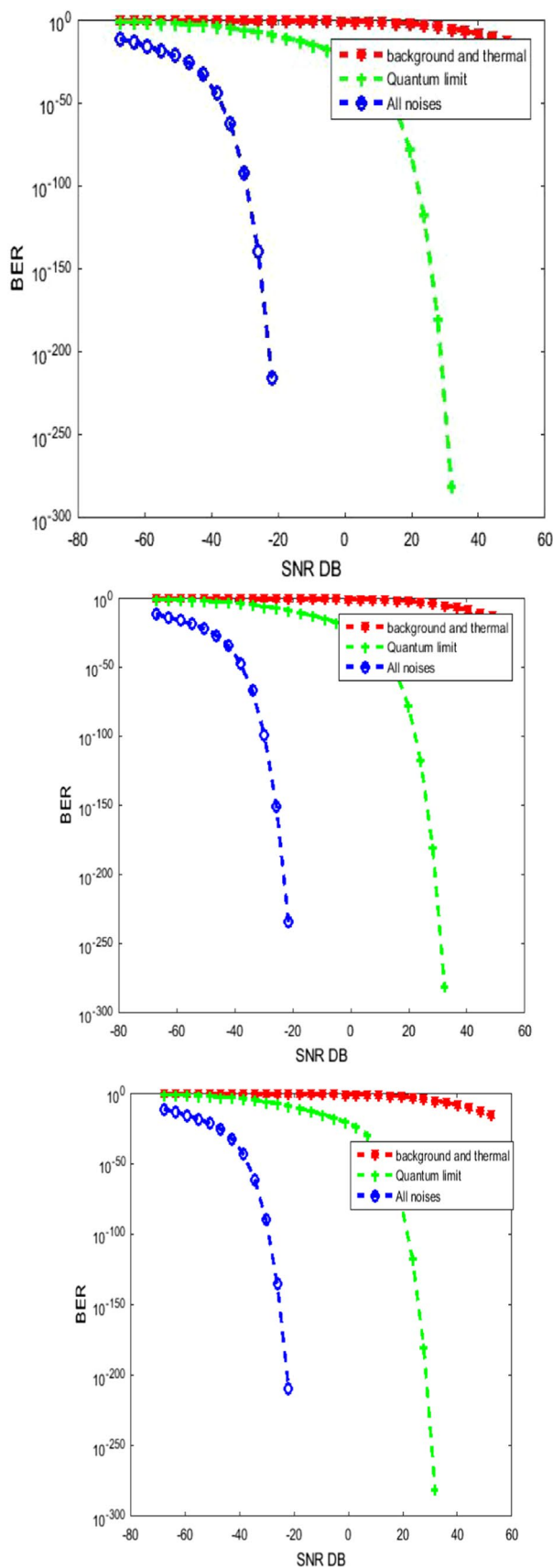


Fig. 7 (continued)

the OOK, BPSK, MPSK, MQAM modulation techniques. It was experimentally verified that the value of BER is greatly affected in the presence of quantum noise and thermal noise. In addition to the effect of atmospheric turbulence in channel, simulated results are explored using the Gauss–Hermite quadratic method [xx] to determine the performance of thermal radiative power under turbulent conditions. The proposed representation is optimum to assess the error probability with the various modulation schemes employed in FSO systems. It was observed that in case of strong turbulence, even a small routing error affects correlation performance, whereas within the case of moderate turbulence effects, the correlation performance degrades. Further investigations revealed that the degradation of FSO system link greatly affected the FSO behavior during common fading conditions as well.

Acknowledgments The authors would like to acknowledge Lendi Institute of Engineering and Technology, Jonnada, Vizianagaram, India for their support of the research work.

Funding The author(s) received no financial support for the authorship, and/or publication of this article.

Declarations

Conflict of interest The authors declare there is no conflict of interest.

References:

1. Bach T. Vu, Ngoc T. Dang, Truong C. Thang, Anh T. Pham, Bit Error rate analysis of rectangular QAM/FSO systems using an APD receiver over atmospheric turbulence channels. *J. Opt. Commu. Network.* **5**(5), 437–446 (2013)
2. R. Kaushik, V. Khandelwal, R.C. Jain, A new closed form approximation for BER for optical wireless systems in weak atmospheric turbulence. *J. Opt. Commu.* **39**(2), 247–253 (2018)
3. Haixing Miao, Nicolas D. Smith, Matthew Evans, Quantum limit for laser interferometric gravitational-wave detectors from optical dissipation. *Phys. Rev. X.* **9**(1), 011053 (2019)
4. R. Kaushik, V. Khandelwal, R.C. Jain, An approximation for ber of optical wireless system under weak atmospheric turbulence using point estimate. *J. Opt. Commu.* **40**(4), 473–479 (2019)
5. Z. Rajbhandari, “*FSO link performance under the effect of atmospheric turbulence optical wireless communications system and channel modelling with MATLAB®* (CRC Press, Francis, 2012)
6. Antonio García-Zambrana, Carmen Castillo-Vázquez, Beatriz Castillo-Vázquez, Alejandro Hiniesta-Gómez, Selection transmit diversity for FSO links over strong atmospheric turbulence channels. *IEEE Photon. Technol. Let.* **21**(14), 1017 (2009)
7. Zixiong Wang, Wen-De. Zhong, Yu. Changyuan, Performance improvement of OOK free-space optical communication systems by coherent detection and dynamic decision threshold in atmospheric turbulence conditions. *IEEE Photon. Technol. Let.* **24**(22), 2035 (2012)
8. Bach T. Vu, Ngoc T. Dang, Truong C. Thang, Anh T. Pham, Bit error rate analysis of rectangular QAM/FSO systems using an

- APD receiver over atmospheric turbulence channels. *J. Opt. Commun. Netw.* **5**(5), 437 (2013)
9. Kostas P. Peppas, P. Takis Mathiopoulos, Free-space optical communication with spatial modulation and coherent detection over h-k atmospheric turbulence channels. *J. Lightwave Technol.* **33**(20), 4221–4232 (2015). <https://doi.org/10.1109/JLT.2015.2465385>
 10. Abir Touati, Abderrazak Abdaoui, Farid Touati, Murat Uysal, Ammar Bouallegue, On the effects of combined atmospheric fading and misalignment on the hybrid FSO/RF transmission. *J. Opt. Commun. Netw.* **8**(10), 710–715 (2016)
 11. Mohammad Ali Amirabadi, Vahid Tabataba Vakili, A new optimization problem in FSO communication system. *IEEE Commun. Lett.* **22**(7), 1442–1445 (2018). <https://doi.org/10.1109/LCOMM.2018.2831710>
 12. Soyinka Nath, Sujata Sengar, Shreesh Kumar Shrivastava, and Shree Prakash Singh, “Impact of Atmospheric Turbulence, Pointing Error, and Traffic Pattern on the Performance of Cognitive Hybrid FSO/RF System.” *IEEE Trans. Cognit. Commun. Network.* **5**(4), 1194 (2019)
 13. Ajanta Barh, Peter Tidemand-Lichtenberg, Christian Pedersen, Thermal noise in mid-infrared broadband upconversion detectors. *Opt. Express.* **26**(3), 3249 (2018)
 14. Z. Xu, G. Xu, Z. Zheng, BER and channel capacity performance of an FSO communication system over atmospheric turbulence with different types of noise. *Sensors* **21**, 3454 (2021). <https://doi.org/10.3390/s211103454>
 15. R. KVIČALA, V. KVIČERA, M. GRÁBNER, O. FIŠER. BER and availability measured on FSO Link. *Radio Eng.* **16**(3), 17–22 (2007)
 16. M. Venkatachalam, P. Loganathan, System stability improvement and cost-effective solution by accelerated distance protection using direct Fiber optic signal. *J. Inst. Eng. (India) Ser. B* **102**(3), 531–537 (2021). <https://doi.org/10.1007/s40031-021-00562-0>
 17. Sonali Chauhan, Rajan Miglani, Lavish Kansal, Gurjot Singh Gaba, Mehedi Masud, Performance analysis and enhancement of free space optical links for developing state-of-the-art smart city framework. *Photonics* **7**(4), 132 (2020). <https://doi.org/10.3390/photonics7040132>
 18. V. Srivastava, A. Mandloi, G.G. Soni, Outage probability and average BER estimation of FSO system employing wavelength diversity. *Opt. Quant. Electron.* **51**, 229 (2019). <https://doi.org/10.1007/s11082-019-1943-4>
 19. H. Singh, N. Mittal, H. Singh, Analysis of Bit error rate performance and atmospheric attenuation coefficient of free space optical (FSO) link. *Int. J. Adv. Sci. Technol.* **29**(10s), 1635–1642 (2020)
 20. S.S. Abdelhak, A.E. Morra, F.E. Abd El-Samie, A.E. Elfiqi, Performance analysis of different intensity modulation techniques over atmospheric turbulent free-space optical channels. *J Opt Soc Am A Opt Image Sci Vis.* **37**(11), C138–C145 (2020)
 21. Shantanu Jagdale, Brijesh Iyer, Sanjay L. Nalbalwar, Shankar B. Deosarkar, Design of high speed multistream free space optics link under clear weather condition. *Int. J. Auton. Comput. (IJAC).* **3**(3/4), 195 (2020)
 22. V.P. Singh, S. Gupta, H. Pasupuleti et al., A methodology to study the effect of smoke and fire on indoor RF propagation. *J. Inst. Eng. India Ser. B.* **100**, 33–39 (2019)

Publisher’s Note Springer Nature remains neutral with regard to jurisdictional claims in published maps and institutional affiliations.

Springer Nature or its licensor holds exclusive rights to this article under a publishing agreement with the author(s) or other rightsholder(s); author self-archiving of the accepted manuscript version of this article is solely governed by the terms of such publishing agreement and applicable law.